Jordan Journal of Civil Engineering, Volume **12**, No. **3**, **2018**

A Numerical Study on Improvement of Shape Memory Alloy Bolt Characteristics of Beam-Column Connections

Mohamed O. Elsawy [1)]***, Atef Eraky*** [2)] ***and Osama Elhusseiny*** [3)]

[1)] Egyptain Russian University, Egypt. E-Mail: iam.elsawy@hotmail.com
[2)] Professor, Zagazig University, Egypt. E-Mail: atef_eraky@yahoo.com
[3)] Zagazig University, Egypt.

ABSTRACT

Before the 1990s, numerous existing buildings, built with steel beam-column connections, needed retrofitting to be safe during the coming earthquakes and withstand dynamic effects in general. The purpose of this research is to improve the unique advantages of shape memory alloy as an alternative material for bolts in steel beam-column connections. Three-dimensional non-linear finite element models of steel beam-column connections are subjected to a load system applied at the tip of the cantilever beam. The study is conducted to examine the effect of changing initial and final transformation stresses of SMA bolts and investigate their impacts on energy dissipation of the joint in flexural behavior.

KEYWORDS: Shape memory alloys, Super-elastic effect, Beam-column connection, Bolts.

INTRODUCTION

In steel buildings, portions of columns that are connected to beams at their intersections are called beam-column joints. Since their constituent materials have limited strengths, the joints have a limited force-carrying capacity. When forces larger than these are applied during earthquakes, joints are severely damaged. Repairing damaged joints is difficult; therefore, damage must be avoided. Thus, the connections between beams and columns have become critical components.

Dabaon et al. classified beam–column connections *via* rigidity (Dabaon et al., 2002; Dabaon, 2010). Evaluation of M- ϕ relation for stiffened and extended steel beam-column end-plate connections is presented by Shi and Mohamadi (Shi et al., 2007; Mohamadi and Mofid, 2011). Numerous investigations on the behavior of traditional connections under monotonic and cyclic loads presented several interpretations about the role of every parameter in the behavoir of the beam – column connection. Dessouki monitored the distribution of stresses in the end plates for different configurations (Dessouki et al., 2013). Faella et al. investigated the dependence of extended end- plate connection (Dessouki et al., 2013) behavior on the geometrical details of the connections (Faella et al., 1997). Flushed end-plate attracted the interest of researchers in comparison with extended end-plate connections (Shaker, 2014).

Parameters like beam depth, end-plate thickness, bolt diameter, bolts inside and outside pitch, inner bolt pitch, bolt gage and end-plate stiffener were taken into account to investigate the extended end-plate moment connections experimentally and analytically (Diaz et al.,

Received on 16/11/2017.
Accepted for Publication on 14/4/2018.

2011; Swanson et al., 2002; Kukreti and Zhou, 2006; Mashaly et al., 2011). Bolt pretension force, initial imperfection, local buckling and modeling of contact between different surfaces were studied by Ismail et al. in a reliable three-dimensional FEM and they compared their results with those of available published experiments (Ismail et al., 2016).

History of using shape memory alloys (SMAs) in construction applications extends back to 1932. SMAs were widely used after 1990, especially after the 1994 Northridge earthquake and the 1995 Kobe earthquake (Clark et al., 1995; Tamai and Kitagawa, 2002; Corbi, 2003; Han et al., 2003; Li et al., 2004; Song et al., 2006). DesRoches and Delemont (2002) presented the results of studying the efficiency of using SMA restrainers to reduce the response of decks in a multi-span simply supported bridge. The superelastic properties of Ni–Ti alloy under cyclic loading and shape memory alloy wires and bars were tested to evaluate the effects of bar size and loading history on strength and equivalent damping (DesRoches et al., 2004; DesRoches et al., 2010; Ocel et al., 2004).

A half-scale interior beam-column connection was designed by Speicher et al. (2011) to assess the feasibility of incorporating super-elastic Ni–Ti alloy in a moment-resisting frame. Sepúlveda et al. (2008) presented the details of an experimental investigation on a prototype partially restrained connection using copper-based shape memory alloy (SMA) bars. Fang et al. (2014) presented a comparison between seven SMA connections and one HS connection. Yam et al. (2015) and Wang et al. (2015) detailed an FE study to take an in-depth look into the behavior of stiffened extended end-plate connections equipped with SMAs.

To overcome difficulties and problems associated with traditional techniques for strengthening beam - column joints, like strengthening beam ribs and column stiffeners, increasing bolt and weld size, corrosion protection and special attachments, this study focused on the use of Shape Memory Alloy (SMA) bolts that may be used as an alternative material for traditional high-strength bolts, so as to carry large rotation due to applied moment. The main objective of this research is to study the flexural response of beam-column connection. The investigation is based on a non-linear finite element analysis to evaluate the influence of main structural parameters on structural performance, which can be achieved by giving a better detail of initial and final transformation stresses for SMA bolts and their effects on energy dissipation of the joint.

THEORY

A shape memory alloy (SMA) is a metallic alloy that "remembers" its original shape. Upon loading and unloading cycles, an SMA can undergo large deformation without showing residual strains (pseudo-elasticity effect, also often called superelasticity) and recover its original shape through thermal cycles (shape memory effect).

Such distinct material behavior is due to the material micro-structure that is divided into two different crystallographic structures; one characterized by austenite (A) and another one by martensite (S). Austenite is the crystallographically more-ordered phase and martensite is the crystallographically less-ordered phase. The key SMA characteristic is the occurrence of a martensitic phase transformation. Typically, the austenite is stable at high temperatures and low stress, while the martensite is stable at low temperatures and high stress.

As shown in Fig.1, the martensite becomes unstable upon unloading and transforms back to austenite with restoring the initial undeformed shape. The recoverable strain of SMAs can be as high as 8%-10%, which is called super-elastic effect (SE) or pseudo-elasticity (PE). Below martensite finish temperature, the material is fully in its martensitic form. Upon loading above a certain strain, the detwinning process of martensite

occurs and the material is easily deformed to several percent strain (Ma et al., 2007).

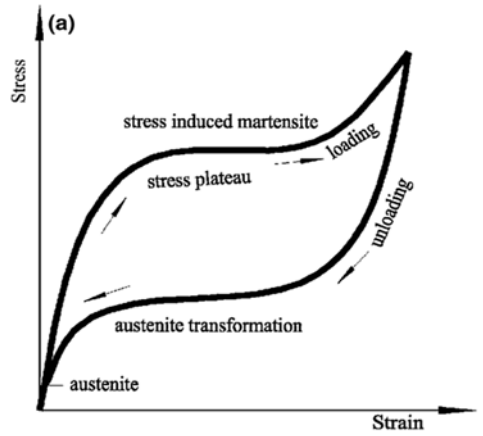

Figure (1): Stress–strain curves for SMAs of pseudo-elasticity effect (PE) (Ma et al., 2007)

As shown in Fig.2, the phase transformation from martensite to austenite starts upon heating the SMA above austenite start temperature, while the phase transformation is complete at austenite finish temperature, resulting in recovering to the initial shape. This is called the shape memory effect (SME) (Ma et al., 2007).

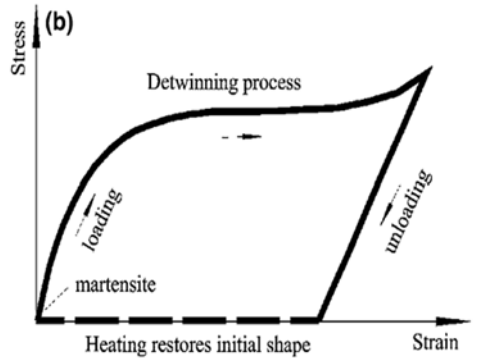

Figure (2): Stress–strain curves for SMAs of shape memory effect (SME) (Ma et al., 2007)

Two of the phase transformations of shape memory alloys are considered here; A to S and S to A. Two internal variables; the martensite fraction (ξ_S) and the austenite fraction (ξ_A), are introduced. ξ_A is a dependent variable and the independent internal variable chosen here is ξ_s. They are assumed to satisfy the relation expressed as:

$$\xi_S + \xi_A = 1 \tag{1}$$

The material behavior is assumed to be isotropic. The pressure dependency of the phase transformation is modeled by introducing the Drucker-Prager loading function, as follows:

$$F = q + 3\alpha p \tag{2}$$

$$q = \sqrt{(3/2\ S : S)} \tag{3}$$

$$S = \sigma - P1 \tag{4}$$

$$P = 1/3\ \sigma : 1 \tag{5}$$

where α is the material parameter, σ is the stress and 1 is the identity tensor. The evolution of the martensite fraction ξ_S is then defined as follows:

$$\xi_s = -H^{AS}(1 - \xi s)\frac{F`}{F - \sigma_f^{AS}(1+\alpha)}$$

A to S Transformation (6)

$$\xi_s = H^{AS}\xi s\frac{F`}{F - \sigma_f^{SA}(1+\alpha)}$$

S to A Transformation (7)

where σ_f^{AS}, σ_f^{SA}, σ_s^{AS} *and* σ_s^{SA} are the material parameters shown in Fig.3. The scalar quantities H^{AS} and H^{SA} are defined by the relations:

$$H^{AS} = \begin{cases} 1 \ if \begin{cases} \sigma_s^{AS}(1+\alpha) < F < \sigma_f^{AS}(1+\alpha) \\ F` > 0 \end{cases} \\ 0 \qquad otherwise \end{cases} \tag{8}$$

$$H^{SA} = \begin{cases} 1 \ if \begin{cases} \sigma_f^{SA}(1+\alpha) < F < \sigma_s^{SA}(1+\alpha) \\ F` < 0 \end{cases} \\ 0 \qquad otherwise \end{cases} \quad (9)$$

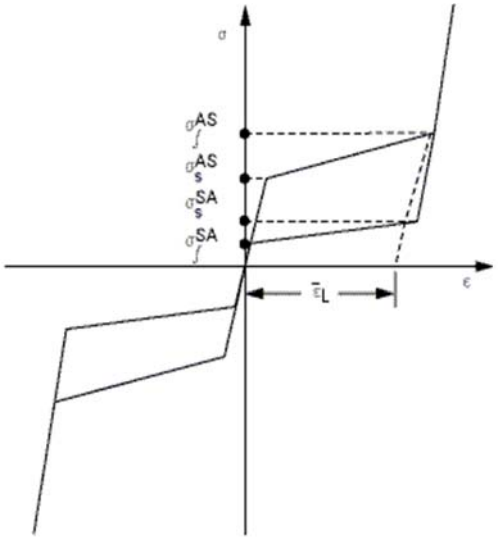

Figure (3): Idealized stress–strain diagram of super-elastic behavior by using the Auricchio's model (Ma et al., 2008)

The material parameter α characterizes the material response in tension and compression. If tensile and compressive behaviors are the same, then α = 0. For a uniaxial tension-compression test, α can be related to the initial value of austenite to martensite phase transformation in tension and compression ($\sigma_c^{AS}, \sigma_t^{AS}$, respectively) as:

$$\alpha = \frac{\sigma_c^{AS} - \sigma_t^{AS}}{\sigma_c^{AS} + \sigma_t^{AS}} \quad (10)$$

The stress-strain relation is:

$$\sigma = D: (\varepsilon - \varepsilon_{tr}) \quad (11)$$

$$\varepsilon_{tr} = \xi \, \varepsilon_L \frac{\partial F}{\partial \sigma} \quad (12)$$

where D is the elastic stiffness tensor, ε_{tr} is the transformation strain tensor and ε_L is the material parameter shown in Fig.3. The SMA defined parameters are summarized in Table 1.

Table 1. Shape memory alloy control parameters

Parameter	Property
σ_s^{AS}	Starting stress value for the forward phase transformation
σ_f^{AS}	Final stress value for the forward phase transformation
σ_s^{SA}	Starting stress value for the reverse phase transformation
σ_f^{SA}	Final stress value for the reverse phase transformation
ε_L	Maximum residual strain
α	Parameter measuring the difference between material responses in tension and compression

FINITE ELEMENT MODELING

Both traditional and SMA beam–column connections are modeled by connecting an extended head plate of a cantilever beam with a column by four rows of two bolts. For simulating the behavior of beam-column connection under cyclic loading , ANSYS 14.5 (Nakasone et al., 2006) is used in the analysis of a traditional model and seven SMA models. The first model presents the connection with traditional bolts as shown in Fig.4 and the other SMA bolts shown in Fig.5 have the same properties of S1. With half 3-D modeling having 10850 elements and 12995 nodes for first model and 21453 elements and 24081 nodes for the other models, the results are compared.

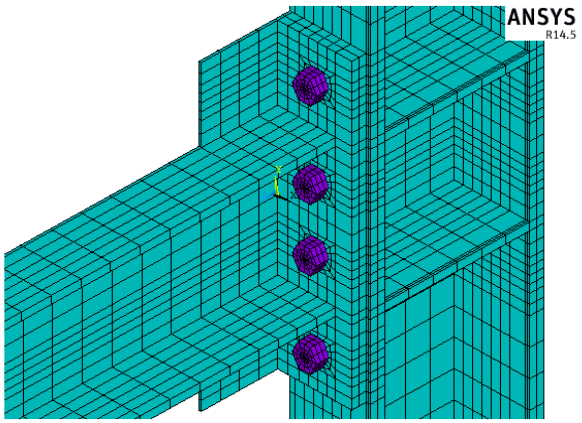

Figure (4): Meshing of half 3D traditional connection

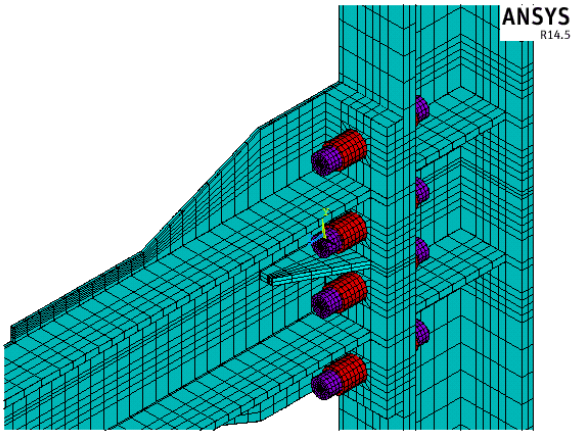

Figure (5): Meshing of half 3D SMA connection

SOLID185 element is used for steel parts and bolts. It is defined by eight nodes having three degrees of freedom at each node: translations in the nodal x, y and z directions. The element has plasticity, hyper-elasticity, stress stiffening, creep, large deflection and large strain capabilities. It also has a mixed formulation capability of simulating deformations of nearly incompressible elasto-plastic materials and fully incompressible hyper-elastic materials. CONTA174 element is used to represent contact and sliding between 3-D surfaces and a deformable surface. TARGE170 element is used to represent various 3-D "target" surfaces for the associated contact element CONTA174.

The shape memory alloy model in ANSYS provides a general capability of modeling bolts in all types of structures using concepts of isotropic elasticity in combination with isotropic tensile and compressive pseudo-elasticity to represent the super-elastic behavior of bolts.

In this study, seven SMA models are used having an H-column ($\frac{200\text{ mm}\times 200\text{ mm}}{12\text{ mm}\times 18\text{ mm}}$) with a height of 900 mm above the beam and 900 mm down the beam and an H-beam with a cross-section of ($\frac{200\text{ mm}\times 150\text{ mm}}{6\text{ mm}\times 10\text{ mm}}$) stiffened by 10 mm thick flange ribs to enhance the rib reinforcement ratio to equal 1.65. Four rows of two bolts (Dia. = 16mm) are arranged as shown in Fig. 6. By installing 35 mm thick washers on both sides of the bolt, the total bolt shank length is 1.2 times that of a normal bolt in the traditional model.

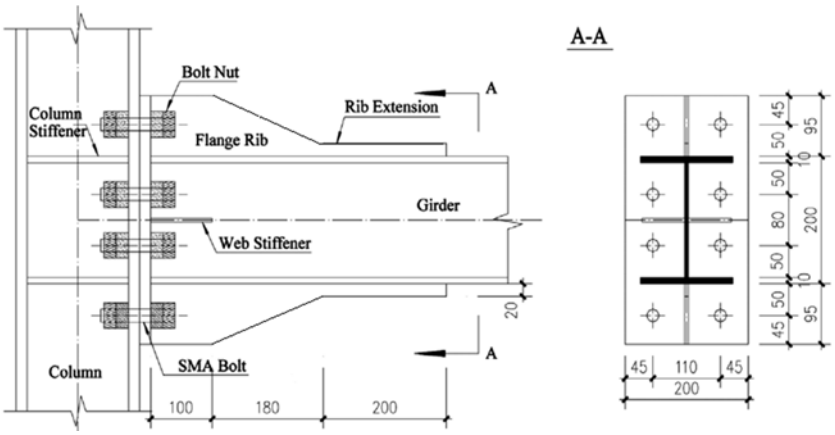

Figure (6): SMA model core dimensions

Based on the material behavior tests, elasto-plastic material behavior with kinematic hardening is selected to simulate material behavior of all components in the FE model. Young's modulus is assumed to be 200000 MPa for all components except for SMA bolts with a Young's modulus of 60000 MPa. The tangential stiffness for all components except for bolts above the yield point was defined as 2% of the initial modulus of elasticity up to 24 ε_y followed by yield stress and ultimate stress of 310 MPa and 460 MPa, respectively. σ_s^{AS} and σ_f^{AS} are equal to 375 MPa and 430 MPa, respectively for SMA bolt material, including shank, head and nut followed by the corresponding transformation stresses in Table 2. To ensure that the connections possess sufficient initial stiffness and recentering capability, an initial prestress of 373 MPa is applied to all SMA bolts. SMA specimens are called type (S) specimens and numbered from 1 to 7.

Table 2. Bolt material properties

Variables of Bolt Material	Specimens						
	S1	**S2**	**S3**	**S4**	**S5**	**S6**	**S7**
σ_s^{SA}, MPa	208	100	100	150	150	175	208
σ_f^{SA}, MPa	138	50	75	100	138	125	100

The effect of changing the reverse phase transformation σ_s^{SA} and final stress value for the reverse phase transformation σ_f^{SA} for SMA bolts on the flexural behavior of beam-column connection is studied in the seven models. Other parameters, such as starting stress value for the forward phase transformation σ_s^{AS}, final stress value for the forward phase transformation σ_f^{AS} and model dimensions, are constant for all tested models. Full bond between flanges, web, stiffeners and ribs is assumed. The column ends are pinned and the beam laterally constrained to avoid lateral torsional buckling. Vertical load is applied at the beam tip simulating dynamic effect on the connection.

RESULTS AND DISCUSSION

A linear variable displacement of the beam flange nodes at a distance of 400 mm from the end plate surface is observed. The connection rotation was determined by dividing the measured linear variable displacement by 400mm. The applied moment was calculated by multiplying the beam reaction force by the cantilever beam length. The entire rotation-moment responses of the two FEA models are shown in Fig.7 and Fig. 8.

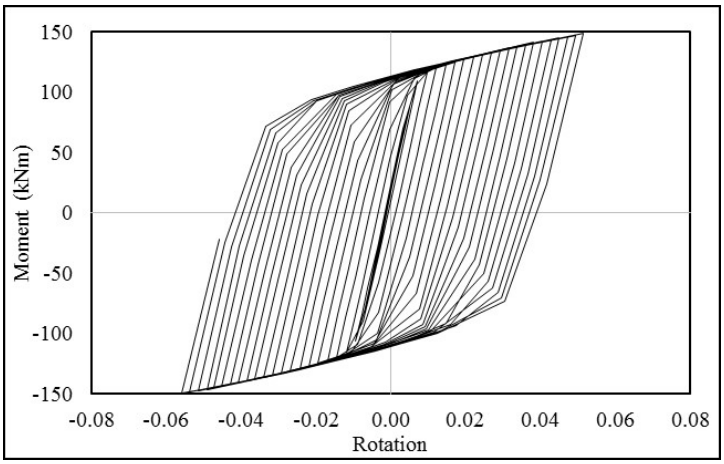

Figure (7): Rotation – moment response of traditional connection

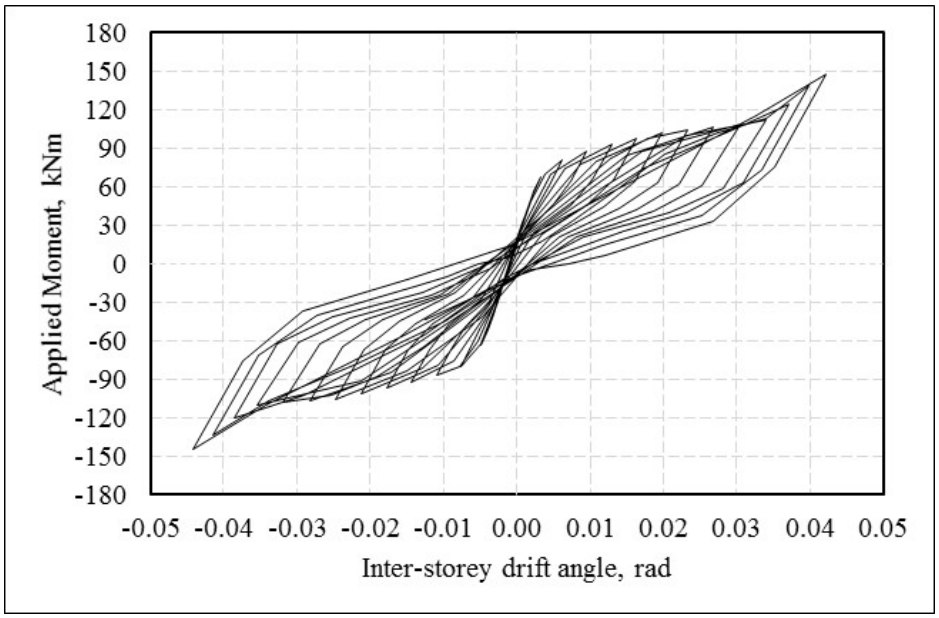

Figure (8): Rotation – moment response of SMA connection

The rotation-applied moment capacity is considered as the base of comparison between the results of the traditional model and the SMA ones. Though the two types of connection have close values of ultimate moment, the SMA connection achieves a rotation of 80% of that of the traditional one.

Table 3 shows maximum plastic rotation (θ_p), ultimate rotation (θ_u), ultimate moment (M_u), equivalent viscous damping (energy dissipation index, ξ_{eq}) and overstrength factor (Ω).

Table 3. Elastic and plastic results of the tested models

Specimen	θ_p, rad	M_u, kNm	θ_u, rad	ξ_{eq}, %	Ω
S1	0.039	147.77	0.044	10.88	1.27
S2	0.036	139.47	0.041	10.68	1.20
S3	0.041	155.40	0.046	12.60	1.34
S4	0.044	155.81	0.050	14.59	1.34
S5	0.054	167.55	0.060	21.08	1.44
S6	0.039	144.37	0.044	10.83	1.24
S7	0.024	115.89	0.028	13.41	0.92

Fig. 9 shows the inter-storey drift angle – applied moment relationship at the last cycle. It is found that S5 has a high total rotation compared with the other models. For the specimen S5, the flexural capacity developed greatly up to a 13.4% increase compared with S1. Specimen S5 achieves the highest ultimate rotation compared with the other models. The value of deformation capacity is almost increased by 36% over that achieved by S1.

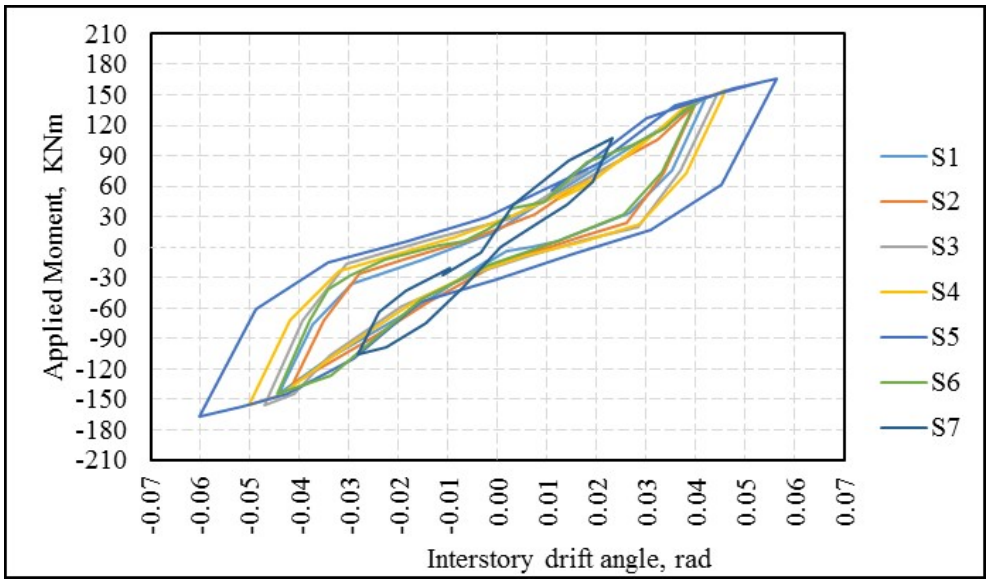

Figure (9): Total rotation-applied moment of last cycle for S1-S7

In general, for connections under dynamic effects, plastic rotations of the connections, which are typical ductility measurements, are usually recorded. For a typical cantilever test system as employed in this study, Fig.10 shows the plastic rotation that can be obtained by deducting the elastic deformation of the beam from the total deformation as given in Charles (2002):

$$\theta_P = \frac{\Delta - P/K_e}{L} \quad (13)$$

where θ_P is the plastic rotation, Δ is the displacement (e.g. beam tip displacement), P is the applied load, K_e is the elastic stiffness of the beam and L is the arm length. It is found that S5 has the highest plastic rotation compared with the other models.

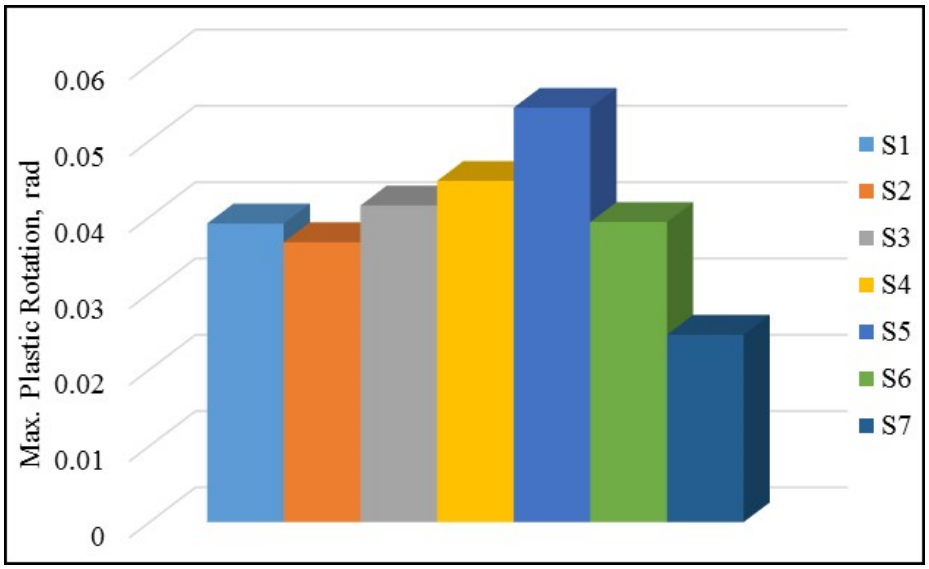

Figure (10): Ultimate plastic rotation for S1-S7

Some structural members are designed to absorb and dissipate the transmitted energy to mitigate overall damages and thus to avoid total collapse. Fig.11 shows the energy dissipation capacities of the SMA connections that are examined here *via* equivalent viscous damping ξ_{eq}, which is defined as (Speicher, DesRoches and Leon, 2011):

$$\xi_{eq} = \frac{W_D}{4\Pi W_E} = \frac{W_D}{2\Pi K_s \theta_{max}^2} \quad (14)$$

where the energy loss per cycle W_D is evaluated as the area enveloped by complete hysteretic cycle, K_s is the secant rotational stiffness in the considered hysteretic cycle, θ_{max} is the maximum deformation (rotation in this study) in the hysteretic cycle and W_E is the energy absorbed in a linear system that has the same maximum rotation and maximum moment. It is found that S5 has the highest energy dissipation compared with the other models, achieving a percentage of almost twice the value in S1.

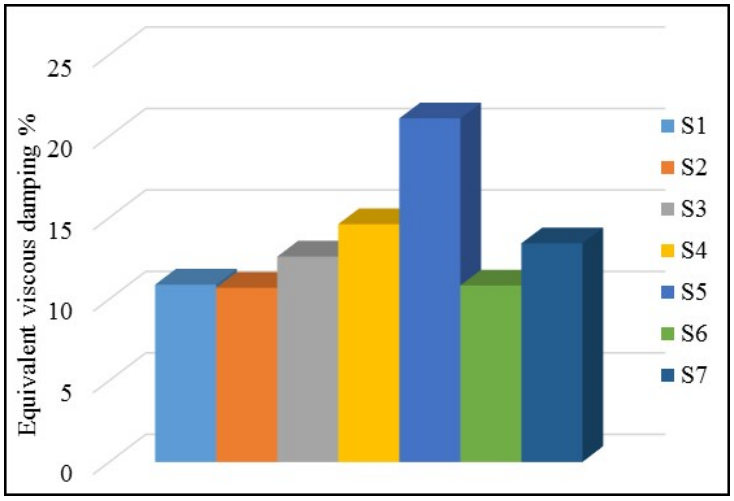

Figure (11): Energy dissipation for S1-S7

Fig. 12 shows the energy loss along the loading time of each model. It is found that S5 has the highest energy loss within time-vertical displacement history compared with the other models.

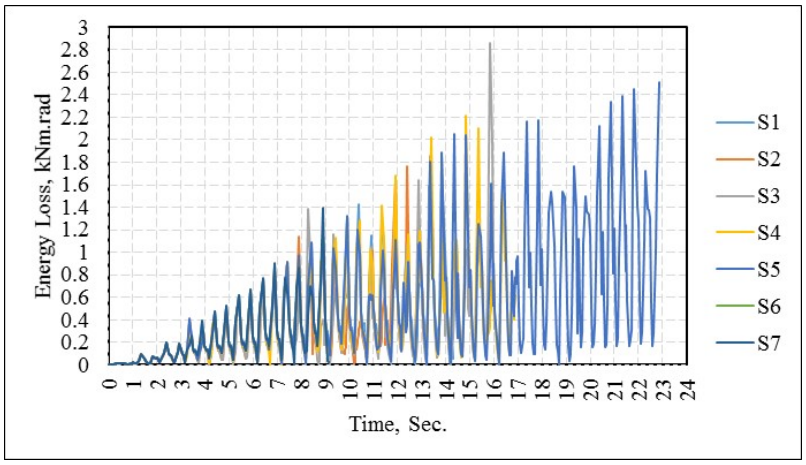

Figure (12): Energy losses for S1-S7

Fig. 13 shows the overstrength factor that is simply defined as the ratio of load value at ultimate moment capacity (M_u) to moment value at yield (M_y). The overstrength factor is slightly increased in S3 and S4 and is 13.4% for S5 over that in S1. It is found that S5 has a higher overstrength factor compared with the other models. Decreasing the value of σ_s^{SA} in S5 rather than S1 while keeping σ_f^{AS} constant gives a chance to increase E^S, thereby increasing the range of plasticity that yields high values of ultimate plastic rotation and moment, thus increasing overstrength factor and increasing time before total collapse.

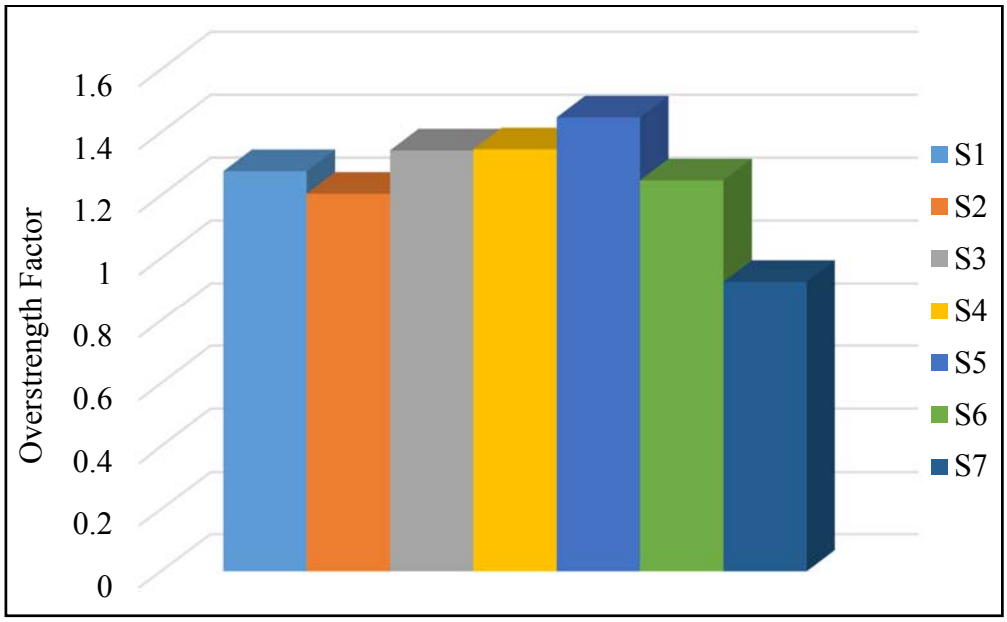

Figure (13): Overstrength factor for S1-S7

CONCLUSIONS

The effect of changing the reverse phase transformation σ_s^{SA} and final stress value of the reverse phase transformation σ_f^{SA} for SMA bolts on the flexural behavior of beam-column connections is studied on seven models. The following major conclusions can be drawn from this study:

1- Using of balanced values of σ_s^{SA} and σ_f^{SA} to keep E^A approximately near to E^S and keep ascending inclination of loading line from σ_s^{AS} to σ_f^{AS} approximately near to descending inclination of unloading line from σ_s^{SA} to σ_f^{SA}, leads to significant improvement in the flexural capacity with high energy dissipation and deformability.

2- Decreasing values of σ_s^{SA} and σ_f^{SA} rather than σ_s^{AS} and σ_f^{AS}, respectively, increases net area under loading and unloading hysteresis curves and so, the more energy dissipation, the better characteristics in the behavior of such connections within dynamic effects.

3- Decreasing value of σ_s^{SA} gives a chance to increase E^S, so increasing the range of plasticity that yields high values of ultimate plastic rotation and moment, thus increasing time before total collapse.

REFERENCES

Charles, R. (2002). "Connection performance for seismic design of steel moment frames". Journal of Structural Engineering, 128, 517-525.

Clark, P., Aiken, I., Kelly, J., Higashino, M., and Krumme, R. (1995). "Experimental and analytical studies of shape-memory alloy dampers for structural control".

Corbi, O. (2003). "Shape memory alloys and their application in structural oscillation attenuation". Simulation Modelling: Practice and Theory, 11, 387-402.

Dabaon, M. (2010). "Fundamentals of steel design course and design tables". Second Edn., Tanta University, Egypt.

Dabaon, M., El-Boghdadi, M., El-Kasaby, E., and Gerges, N. (2002). "Early prediction of initial stiffness of composite joints". Regional Conference on Civil Engineering Technology and International Symposium on Enviromental Hydrology. Cairo: American Society of Civil Engineers.

DesRoches, R., and Delemont, M. (2002). "Seismic retrofit of simply supported bridges using shape memory alloys". Engineering Structures, 24, 325-332.

DesRoches, R., McCormick, J., and Delemont, M. (2004). "Cyclic properties of superelastic shape memory alloy wires and bars". Journal of Structural Engineering, 130, 38-46.

DesRoches, R., Taftali, B., and Ellingwood, B. (2010). "Seismic performance assessment of steel frames with shape memory alloy connections; part I: analysis and seismic demands". Journal of Earthquake Engineering, 14, 471-486.

Dessouki, A., Youssef, A., and Ibrahim, M. (2013). "Behavior of I-beam bolted extended end-plate moment connections". Ain Shams Engineering Journal, 4, 685-699.

Díaz, C., Victoria, M., Marti, P., and Querin, O. (2011). "FE model of beam-to-column extended end-plate joints". Journal of Constructional Steel Research, 67, 1578-1590.

Faella, C., Piluso, V., and Rizzano, G. (1997). "A new method to design extended end plate connections and semi-rigid braced frames". Journal of Constructional Steel Research, 41, 61-91.

Fang, C., Yam, M., Lam, A., and Xie, L. (2014) "Cyclic performance of extended end-plate connections equipped with shape memory alloy bolts". Journal of Constructional Steel Research, 94, 122-136.

Han, Y., Li, Q., Li, A., Leung, A., and Lin, P. (2003). "Structural vibration control by shape memory alloy dampers". Earthquake Engineering and Structural Dynamics, 32, 483-499.

Ismail, R., Fahmy, A., Khalifa, A., and Mohamed, Y. (2016). "Numerical study on ultimate behaviour of bolted end-plate steel connections". Latin American Journal of Solids and Structures, 13, 1-22.

Kukreti, A., and Zhou, F. (2006). "Eight-bolt end-plate connection and its influence on frame behavior". Engineering Structures, 28, 1483-1493.

Li, H., Liu, M., and Ou, J. (2004). "Vibration mitigation of a stay cable with one shape memory alloy damper". Structural Control and Health Monitoring, 11, 21-36.

Ma, H., Cho, C., and Wilkinson, T. (2008). "A numerical study on bolted end-plate connection using shape memory alloys". Materials and Structures, 41, 1419-1426.

Ma, H., Wilkinson, T., and Cho, C. (2007). "Feasibility study on a self-centering beam-to-column connection by using the superelastic behavior of SMAs". Smart Materials and Structures, 16, 15-55.

Mashaly, E., El-Heweity, M., Abou-Elfath, H., and Osman, M. (2011). "Behavior of four-bolt extended end-plate connection subjected to lateral loading". Alexandria Engineering Journal, 50, 79-90.

Mohamadi, S., and Mofid, M. (2011). "New modeling for moment–rotation behavior of bolted endplate connections". Scientia Iranica, 18, 827-834.

Nakasone, Y., Yoshimoto, S., and Stolarski, T. (2006). "Engineering analysis with ANSYS software". Oxford, UK: Elsevier's Science and Technology.

Ocel, J., DesRoches, R., Leon, R., Hess, W., Krumme, R., and Hayes, J. et al. (2004). "Steel beam-column connections using shape memory alloys". Journal of Structural Engineering, 130, 732-740.

Sepúlveda, J., Boroschek, R., Herrera, R., Moroni, O., and Sarrazin, M. (2008). "Steel beam–column connection using copper-based shape memory alloy dampers". Journal of Constructional Steel Research, 64, 429-435.

Shaker, F. Abd Elrahman. (2014). "Analytical behavior of steel pre-tensioned bolted connections with flushed and extended end-plates under bending". World Applied Sciences Journal, 30 (6), 673-684.

Shi, Y., Shi, G., and Wang, Y. (2007). "Experimental and theoretical analysis of the moment–rotation behaviour of stiffened extended end-plate connections". Journal of Constructional Steel Research, 63, 1279-1293.

Song, G., Ma, N., and Li, H. (2006). "Applications of shape memory alloys in civil structures". Engineering Structures, 28, 1266-1274.

Speicher, M., DesRoches, R., and Leon, R. (2011). "Experimental results of a Ni-Ti shape memory alloy (SMA)-based recentering beam-column connection". Engineering Structures, 33, 2448-2457.

Swanson, J., Kokan, D., and Leon, R. (2002). "Advanced finite element modeling of bolted T-stub connection components". Journal of Constructional Steel Research, 58, 1015-1031.

Tamai, H., and Kitagawa, Y. (2002). "Pseudo-elastic behavior of shape memory alloy wire and its application to seismic resistance members for buildings". Computational Materials Science, 25, 218-227.

Wang, W., Chan, T., and Shao, H. (2015). “Numerical investigation on I-beam to CHS column connections equipped with Ni-Ti shape memory alloy and steel tendons under cyclic loads". Structures: Elsevier, 114-124.

Yam, M., Fang, C., Lam, A., and Zhang, Y. (2015). "Numerical study and practical design of beam-to-column connections with shape memory alloys". Journal of Constructional Steel Research, 104, 177-192.